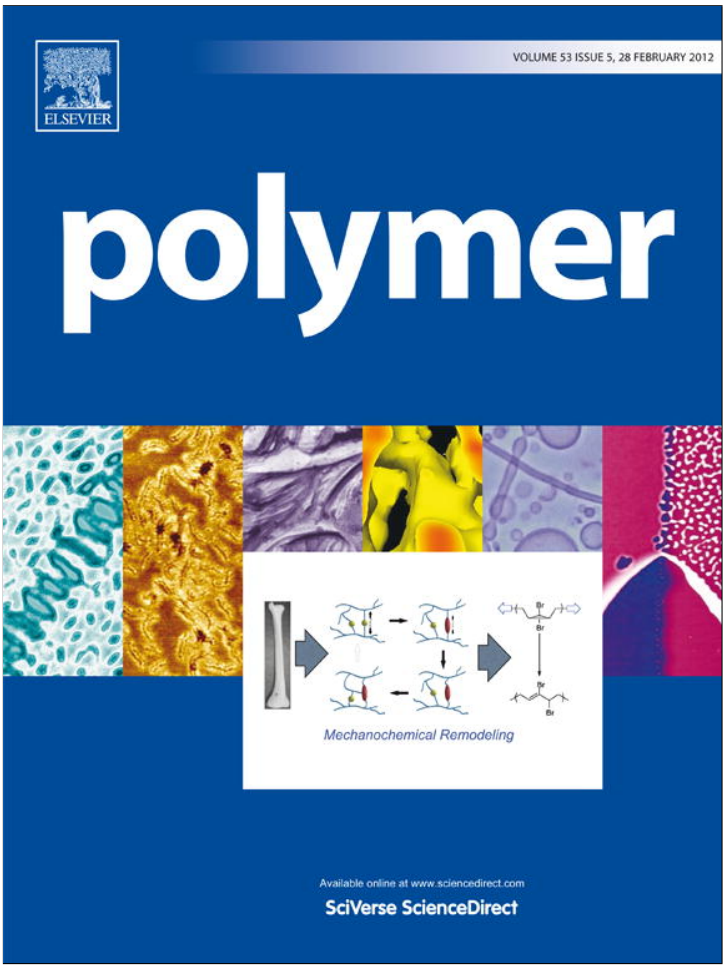

Polymer 53 (2012) 1098–1108

Contents lists available at SciVerse ScienceDirect

Polymer

journal homepage: www.elsevier.com/locate/polymer

Transformation of waterborne hybrid polymer particles into films: Morphology development and modeling

Monika Goikoetxea [a], Yuri Reyes [a], Carolina M. de las Heras Alarcón [b], Roque J. Minari [a], Itxaso Beristain [a], María Paulis [a], María J. Barandiaran [a], Joseph L. Keddie [b], José M. Asua [a,*]

[a] Institute for Polymer Materials, POLYMAT, Departamento de Química Aplicada, University of the Basque Country (UPV/EHU), Centro Joxe Mari Korta, Avenida Tolosa 72, 20018 Donostia-San Sebastián, Spain
[b] Department of Physics, University of Surrey, Guildford, Surrey GU2 7XH, UK

ARTICLE INFO

Article history:
Received 26 August 2011
Received in revised form
11 January 2012
Accepted 14 January 2012
Available online 20 January 2012

Keywords:
Alkyd/acrylic nanocomposites
Particle and film morphology
Mathematical simulation

ABSTRACT

Films cast from multiphase polymer particles have the potential to combine the properties of their components synergistically. The properties of the film depend on the hybrid polymer architecture and the film morphology. However, how the polymer microstructure and particle morphology are transformed during film formation to determine the film morphology is not well understood. Here, using waterborne alkyd-acrylic nanocomposite particles in a case study, it was found that phase migration leading to the formation of aggregates occurred during film formation. A coarse-grained Monte Carlo model was developed to account for the effects of polymer microstructure and particle morphology on the morphology of the film. The model was validated by comparing its predictions with the observed effects, and then used to explore combinations of polymer microstructure and particle morphology not attainable with the system used as a case study. Significantly, the compatibility of the phases was found to have a greater influence than the morphology of the particles in determining the film structure.

1. Introduction

Synthetic latexes are mainly used in applications (e.g., paints, adhesives, paper and coatings) that require the formation of a film [1–3]. For latexes composed of homogeneous particles, film formation is described as consisting of three main processes [4–7]: (i) evaporation of water to achieve the close-packing of particles, (ii) deformation of particles to fill all the void space, and (iii) interdiffusion of the polymer across particle interfaces to fuse particle boundaries. However, very often these films need to satisfy contradictory requirements, especially in their mechanical properties, and homogenous latexes can hardly fulfill the antagonist application requirements. For instance, binders for coatings are required to have a low minimum film formation temperature (MFFT) to be applied outdoors over a wide range of temperatures. This requires that the glass transition temperature, T_g, of the polymer is below the temperature at which the film is going to be formed. On the other hand, coatings also require a high hardness level that cannot be provided by a low T_g polymer. One solution is to add a coalescing agent [8] to plasticize a polymer with a T_g above the application temperature. The coalescent decreases the MFFT to a level desired for perfect film formation. After the application of the film on a substrate, the coalescent evaporates and the hard polymer remains, but the emission of the coalescent into the atmosphere causes environmental pollution [9]. One way to overcome this problem is to blend two latexes of different T_g value [10–15]. The lower T_g polymer can form a film at a low temperature (low MFFT) and the higher T_g polymer can provide film hardness. However, blending often leads to uneven distribution of the two polymers in the film, which in turn results in haze and low gloss.

A more uniform distribution of the two phases in the film can be achieved by using heterogeneous polymer particles, in which two or more different polymers are simultaneously present in one particle [16–18]. This allows the achievement of film properties not accessible by physically blending different polymer dispersions [8,19]. Implicit in those works is the idea that the film morphology, which determines the film properties, is determined by the particle morphology. However, a general framework of understanding of how the particle morphology translates into film morphology is not available.

There have been a few previous experimental studies to correlate the morphology of particles and films. Gerharz et al. [20] found that in the presence of a good solvent, homogeneous films were formed from composite particles. Schellenberg et al. [21] investigated the morphology of films cast from soft-core/hard-shell

* Corresponding author. Tel.: +34 9 43 018 181; fax: +34 9 43 212 236.
E-mail addresses: jm.asua@ehu.es, jmasua@sq.ehu.es (J.M. Asua).

0032-3861/$ – see front matter © 2012 Elsevier Ltd. All rights reserved.
doi:10.1016/j.polymer.2012.01.021

particles and found that the particle structure inverted during film formation yielding a continuous matrix of soft polymer. Crosslinking of the hard shell avoided film formation. Schuler et al. [8] and Hagen et al. [22] found that the morphology of the particles was preserved during film formation. Lee et al. [23] found that multilayered, slightly crosslinked nanostructured particles led to a nanocomposite film containing domains of both polymers interconnected by their diffuse polymer mixtures. Otts et al. [24] reported on the effect of the synthetic method on film morphology, but experimental evidence of the morphology of the particles was not provided. The behavior of composite particles during film formation could potentially be mimicked by using blends, but the evidence available is that these systems lead to a substantial phase separation [25,26]. In this context, it is clear that a mathematical model aimed at predicting the effect of the polymer microstructure and particle morphology on the film morphology would be highly valuable, but no such model has been reported in the literature. There is a need to establish general principles.

In this work, the effect of polymer microstructure and particle morphology on film morphology was investigated experimentally, and a model was developed to describe and interpret the results. Waterborne alkyd/acrylic hybrids were used as a case study. Alkyd/acrylic hybrids have the potential to out-perform classical soft polymer/hard polymer composite latexes in terms of the balance between low MFFT and hardness of the film. The reason is that the soft alkyd resin reduces the MFFT, and upon film formation, it hardens by autoxidative curing [27].

The synthesis of waterborne alkyd/acrylic hybrids has been extensively studied [28–31] and strategies for the control of the particle morphology, which benefit from the knowledge developed for other polymer/polymer systems [32–37], are available [38]. The effect of the particle morphology on the autoxidative drying rate was reported [39], and recently, the effect of the type of alkyd resin and the compatibilization degree among phases on the mechanical properties of the film, was assessed [40]. However, the effect of the polymer microstructure and particle morphology of alkyd/acrylic hybrids on film morphology has not been studied.

Waterborne alkyd/acrylic hybrids with three different morphologies (i) alkyd in the core and acrylic in the shell, (ii) hemispherical and (iii) acrylic in the core covered by an alkyd resin shell were synthesized. These hybrids had different polymer microstructures in terms of the relative fractions of free acrylic chains, acrylic-alkyd graft copolymer and free alkyd resin. The morphology of the films cast from them was compared to that of the film cast from blends of alkyd and acrylic dispersions. A coarse-grained Monte Carlo model able to account for the effect of polymer microstructure and particle morphology on the morphology of the film was developed. The model was validated by comparing its predictions with the observed effects. It was subsequently used to explore combinations of polymer microstructure and particle morphology that are otherwise difficult to obtain with the system used in the case study.

2. Experimental

Alkyd/acrylic particles with widely different morphologies (alkyd in the core and acrylic in the shell, hemispherical and acrylic in the core partially covered by alkyd resin) were synthesized by miniemulsion polymerization [38]. The solids content was 50 wt% and the alkyd/acrylic ratio was 50/50 wt/wt% in all cases. Particle morphology depends on the interplay between thermodynamics and kinetics [32,34,36,37]. Thermodynamics determines the particle morphology at equilibrium according to the minimum surface energy, and kinetics determines whether the particle reaches the equilibrium morphology or it remains in a metastable (kinetically stable) morphology. Because of the plasticizing effect of the alkyd resin, equilibrium morphologies are usually reached for alkyd/acrylic system [38]. The surface energy is the product of the interfacial area and the interfacial tensions. Therefore, the equilibrium morphology strongly depends on the interfacial tensions. In this work, the interfacial tensions between the alkyd resin and the other phases (acrylic polymer and water) were varied by using two alkyd resins (supplied by Nuplex Resins) with different hydrophilicity: SETAL 293-XX (S293), which is hydrophobic (acid value = 11 mg KOH/g) and the more hydrophilic SETAL 1630WP-292 (S1630, acid value = 21.5 mg KOH/g). In addition, the interfacial tension between the polymers was modified through both the resin and the acrylic degree of grafting. The resin degree of grafting (RDG) is the fraction of the alkyd resin that is grafted to the acrylic polymer. The acrylic degree of grafting (ADG) is the fraction of the acrylic polymer that is grafted to the alkyd resin. Methods to determine RDG and ADG have been reported [41].

Usually, the acrylic chains are substantially longer than the alkyd ones, and therefore most of the acrylic chains contain some alkyd grafted (i.e., ADG is high), whereas only a fraction of the alkyd is grafted to the acrylic polymer, namely, the majority of the alkyd is not grafted [38] (i.e., RDG is usually low). RDG can be increased by maintaining the alkyd resin and the acrylic polymer in close vicinity (hydrophobic resins give higher RDG than hydrophilic ones), using initiators that generate radicals active in hydrogen abstraction (e.g., tert-butyl hydroperoxide, TBHP/ascorbic acid, AsAc, which yields oxygen-centered radicals and hydrophobic enough to readily enter into the polymer particles) [42], and using monomers of different reactivity with the double bonds of the alkyd resin (e.g., acrylates are more reactive than methacrylates) [31]. Therefore, in order to prepare particles of different morphology, the type of resin, the monomer system and the type of initiator were varied. The formulations are summarized in Table 1. The reactions were carried out by batch miniemulsion polymerization following the procedure given elsewhere [38].

Two different redox initiators (TBHP/AsAc, and H_2O_2/FF7) were used to achieve low residual monomer content throughout an additional post-polymerization step, following the procedure described in Ref. [42]. Table 1 also includes the main characteristics of the hybrids prepared. Based on the measurements of the acrylic

Table 1
Summary of the polymerization conditions of used and the characteristics of the hybrids.

Sample (resin type)	Monomer (%wt)	T (°C)	Initiator (Pol. (%wbm)[a]//Post-Pol. (%wbrm)[b])	dp[c] (nm)	ADG (%)	RDG (%)	Pure acrylic (%)	Hybrid polymer (%)	Pure alkyd (%)
S1 (S293)	BA/MMA/SA/AA 47.6/47.6/3.8/0.95	70	V59 (1.6)//TBHP/AsAc (0.25/0.125)	105	89	44	5.5	66.5	28
S2 (S293)	BMA/MMA/SA/AA 47.6/47.6/3.8/0.95	90	V59 (1.6)//H2O2/FF7 (0.25/0.25)	135	100	18	0	59	41
S3 (S1630)	BA/MMA/SA/AA 47.6/47.6/3.8/0.95	70	KPS (1.6)//TBHP/AsAc (0.33/0.165)	88	40–60	21	25	35.5	39.5

All the samples were prepared with 6% weight based on organic phase of Dowfax 2A1 surfactant.
[a] Weight percent of initiator based on monomer used in the polymerization step.
[b] Weight percent of initiator based on residual monomer present at the beginning of the post-polymerization step.
[c] Particle diameter; BA, butyl acrylate; BMA, butyl methacrylate; MMA, methyl methacrylate; SA, stearyl acrylate; AA, acrylic acid; V59, 2,2-azobis(2-methylbutyronitrile); KPS, Potassium persulfate; FF7, Brugolitte FF7.

and the resin degree of grafting, the mass fraction of the total hybrid polymer was estimated as follows:

$$\text{Hybrid polymer} = \text{ADG}\cdot p_A + \text{RDG}\cdot p_R \quad (1)$$

where p_A and p_R are the mass fractions of the acrylic polymer and alkyd resin, respectively, in the dried sample given by:

$$p_A = \frac{\text{mon}\cdot X}{\text{mon}\cdot X + \text{alk} + \text{I} + \text{E}} \quad (2)$$

$$p_R = \frac{\text{alk}}{\text{mon}\cdot X + \text{alk} + \text{I} + \text{E}} \quad (3)$$

where mon is the acrylic monomer, X is the acrylic conversion, alk, the alkyd, I is the initiator content in the formulation and E is the amount of emulsifier used.

The weight percentage of acrylic that remains ungrafted (pure acrylic) and the amount of ungrafted alkyd (pure alkyd) over the total polymer are also given in Table 1.

The morphology of the particles was determined by means of transmission electron microscopy, TEM, using a TECNAI G^2 20 TWIN (200 kV, LaB6), after positively staining them with OsO_4 and negatively staining them with phosphotungstenic acid (PTA). This enhanced the contrast between the alkyd resin (darker, through reaction of the double bonds of the alkyd with the OsO_4) and the acrylic polymer (lighter). The surfaces of the particles were also contrasted.

Both atomic force microscopy (AFM) and transmission electron microscopy (TEM) were used to study the nanostructure of alkyd/acrylic nanocomposite films. Films for AFM analysis were cast on poly(propylene) (PP) sheets with a 40 μm spiral applicator and allowed to dry overnight at a temperature of 22 ± 1 °C and a relative humidity of 55 ± 1% (resulting in a dried film thickness of about 20 μm). All films were rinsed with deionized water prior to AFM analysis.

AFM images were obtained using an atomic force microscope (NTEGRA, NT-MDT, Moscow, Russia) in intermittent contact mode, and with a non-contact "golden" silicon cantilever NT-MDT equipped with conical silicon tip having a radius of curvature less than 10 nm. The nominal resonant frequency f_o of the cantilever was about 115–150 kHz and its spring constant k was about 10 N/m. Parameters needed to describe the tapping conditions are the "free" amplitude A_o (corresponding to oscillation in air), which was fixed at 233 nm, and the setpoint amplitude A_{sp} (corresponding to the amplitude when the tip is in contact with the sample surface) which was kept at 100 nm. The A_{sp}/A_o ratio was equal to 0.43 for all measurements.

For TEM characterization, the films were dried at a temperature of 22 ± 1 °C and a relative humidity of 55 ± 1%. Some of the BMA-based films were also dried at 60 °C due to the higher T_g of this system (the T_g of the BMA is around 20 °C, whereas the T_g of the BA is around −54 °C) [43]. Then, small pieces of the film were cut with a blade and 0.5 mL of a 4 wt% solution (in water) of osmium tetroxide was added. Samples were allowed to react over 7 days with the stain. After staining, an ultracryomicrotome (LEICA EM UC) with cryochamber (LEICA EM FC6) was used to obtain slices of 100 nm that were collected on a copper grid.

For the sake of comparison of film morphologies, blends were made from an all-acrylic latex and emulsions of each of the two alkyd resins. In order to prepare the emulsions, the alkyd resin and an aqueous solution of Dowfax 2A1 (1.8 wt%) were mixed together and magnetically stirred for 20 min. The resulting coarse emulsion was sonified (Branson 450) for 15 min (power 9 and 80% duty cycle). The emulsion was treated (6 cycles) with a Niro-Soavi high-pressure homogenizer with pressures of 410 and 41 bar in the first and second stage valves, respectively. The average alkyd droplet size was 900 nm for the S293 resin and 640 nm for the S1630 resin. Blends of the resin emulsions with an all-acrylic latex in a 1:1 ratio by weight were then prepared. This acrylic latex was made from BA and MMA in a 1:1 weight ratio and synthesized as reported previously [44].

3. Results and discussion

Fig. 1 presents the morphology of the composite particles obtained from TEM analysis. Hybrid S1 synthesized with the hydrophobic resin had an alkyd rich dark core and an acrylic lighter shell, which agrees well with the equilibrium morphology predicted using the interfacial tensions measured for pure polyacrylates MMA/BA/SA/AA (1), alkyd resin SETAL 293 (2) and water (3): $\gamma_{13} = 20$ mN/m and $\gamma_{23} = 33$ mN/m [38]. The actual value of γ_{12} is unknown, although a low value is expected due to the existence of a large amount of grafted copolymer. Hybrid S2 was also prepared with the hydrophobic resin, but a lower extent of the grafting was achieved by using only methacrylate monomers and H_2O_2/FF7 as the post-polymerization initiator system. Methacrylates are less active than acrylates in the reaction with the double bonds of the alkyd resin. On the other hand, the hydroxyl radicals produced by the initiator system are rather hydrophilic and, in order to enter into the polymer particles, they react with monomer in the aqueous phase to yield hydrophobic oligoradicals. These are carbon centered radicals, which are less efficient than the oxygen-centered ones for hydrogen abstraction. It is worth pointing out that hydroxyl radicals may directly enter the polymer particles, but in the presence of monomer the contribution of this process to the overall radical entry rate is negligible [45]. The resulting lower grafting yielded a value of γ_{12} larger than for hybrid S1, leading to the prediction of a hemispherical morphology consisting of alkyd-rich and acrylic-rich phases, which is in agreement with the morphology observed by TEM.

Hybrid S3 was synthesized using a more hydrophilic resin (S1630). Fig. 1 shows that the resin (appearing as small particulates) spread around the polymer particles. This means that the alkyd resin was in the exterior of the particles, but it cannot be concluded whether it was previously forming a partial or a complete shell.

Fig. 2 presents AFM images (both height and phase) of the surface of the films cast from the blends of acrylic and alkyd (hydrophobic and hydrophilic) dispersions. The first column depicts the topography (height image) of the sample and the second column shows the phase shift [46]. The different mechanical and viscoelastic properties of the film are primarily reflected in the phase images. When the tip interacts with a viscous component, more energy is dissipated in comparison to interaction with a more elastic region [47]. In the images presented here, regions that dissipate a greater energy appear darker [48]. The alkyd is a liquid-like low molecular weight compound, whereas the acrylic has a higher elastic modulus [40]. It is worthy pointing out that the films were cast without using a catalyst, that is often used to promote the autoxidative curing of the alkyd, and therefore as the crosslinking rate is slow, the alkyd remained liquid-like [27]. Therefore, when the tip interacts with the alkyd resin, it dissipates more energy than when it interacts with the acrylic. Fig. 2 shows that the large domains of alkyd resin (dark domains), which are substantially greater than the size of the alkyd droplets in the dispersion, were formed. This indicates that the alkyd droplets underwent some coalescence to create a coarser phase distribution. On the other hand, the acrylic particles (brighter) largely kept their identity and appeared surrounded by the alkyd, especially in the case of the hydrophilic resin blend. The film surface of the hydrophilic alkyd/acrylic blend appears richer in the alkyd phase than the

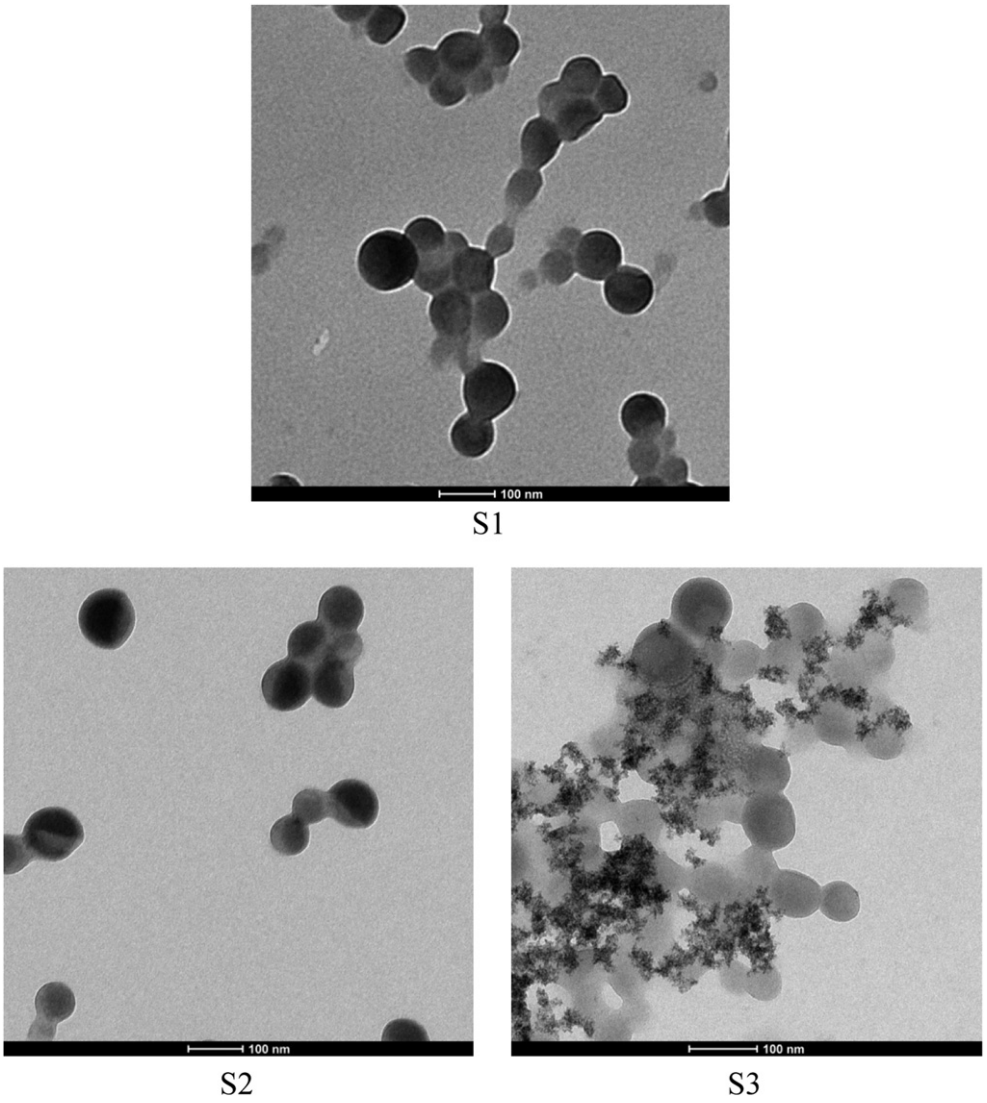

Fig. 1. TEM micrographs of the composite particles with different morphologies. Scale bar 100 nm. Dark regions correspond to the alkyd rich phase and bright regions to the acrylic-rich phase.

hydrophobic blend. This suggests a higher tendency of the hydrophilic resin to migrate to the air surface.

Fig. 3 presents the AFM images of the surface of the films cast from hybrids S1, S2 and S3. In all cases, the particle boundaries are not apparent, which indicates that the particles have coalesced. By comparison, the acrylic particles did not coalesce when blended with alkyd dispersions (*cf*. Fig. 2). In the phase image of the S1 film, there are small domains (typically smaller than the particle size) that appear darker in the images and can reasonably be attributed to the alkyd phase. These domains appear lower in the height image. The S1 particles have an alkyd rich core (Fig. 1). One interpretation of the images is that the AFM tip is penetrating the acrylic shell and detecting the alkyd core, but the possibility of some alkyd leaking from the particles cannot be ruled out. A higher fraction of the darker domains in the phase images is observed at the surface of hybrid S2. Hybrid S3 shows an even higher fraction of the darker phase, which is likewise interpreted as being composed of alkyd. For hybrids S2 and S3, the mean size of these alkyd domains is much greater than that of the polymer particles (135 nm and 88 nm, respectively). Hence, it is inferred that free alkyd resin that is out and/or partially surrounding the particles has migrated to create larger domains. The alkyd aggregates formed in the S3 film are larger than those formed in the S2 film. Furthermore, the size of the alkyd aggregates formed in these hybrid films is smaller than those formed in the films cast from the alkyd/acrylic blends (Fig. 2).

The images presented in Figs. 2 and 3 are obtained from the surface of the film. However, the morphology of the surface may be different from that of the interior of the film. Therefore, cross-sections of the films cast with hybrids S1 and S3 (the hybrid systems showing stronger differences in the morphology of the film surface) were analyzed by TEM (Fig. 4). In these images, the lighter parts correspond to regions rich in acrylic polymer and the dark parts to regions rich in alkyd resin. The black dots might correspond to fractions of the alkyd resin in which the staining agent accumulates (the alkyd resin is not homogenous in composition). Even under these circumstances, Fig. 4 clearly shows that relatively large aggregates of alkyd resin and acrylic polymer were formed in the bulk of the film cast with hybrid S3, whereas a substantially finer dispersion was obtained for hybrid S1.

Figs. 1, 3 and 4, show that the morphology of the films depended on the polymer microstructure and morphology of the particles, and that there was a phase separation and migration to form

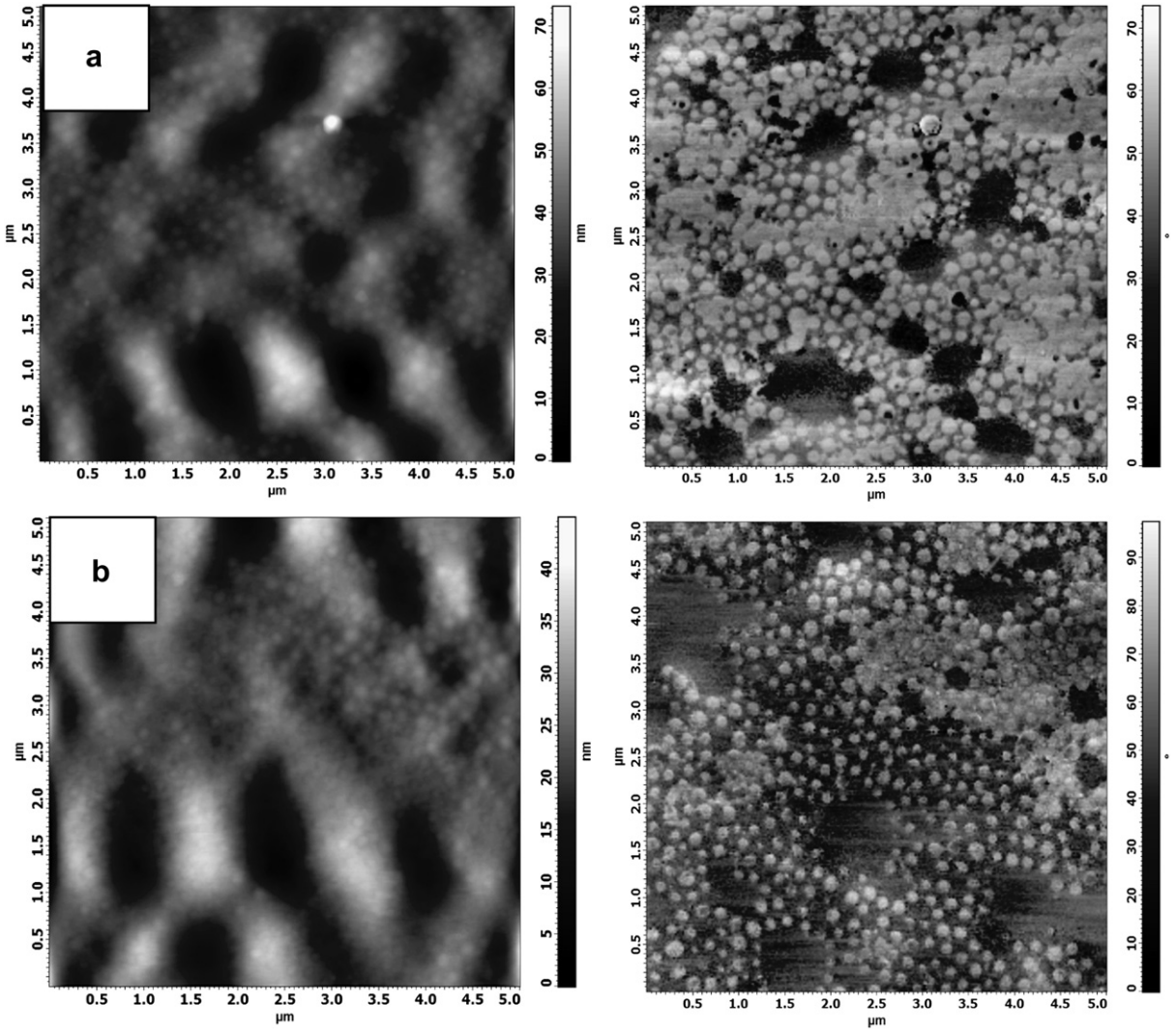

Fig. 2. AFM images obtained from the surfaces of the films cast from blends of the acrylic latex and alkyd-in-water emulsions (a) for the hydrophobic S293 resin and (b) for the hydrophilic S1630 resin. Height images are shown on the left and phase images are shown on the right. All images are 5 μm × 5 μm. Dark regions correspond to the alkyd phase and bright regions to the acrylic phase.

domains that were larger than the size of the phases within the original composite particles.

The moment in which the phase migration occurred is not well defined, but one may speculate that because the morphology of the waterborne hybrid particles was at thermodynamic equilibrium, they were not subjected to any significant driving force for phase migration while they were surrounded by water. Therefore, it seems reasonable to assume that phase migration occurred after water evaporation had been completed. In the absence of water, the driving force for phase migration is the minimization of the surface energy associated with the interfaces between the different phases. In the films cast from the blends there were only two phases: acrylic polymer and alkyd resin, and the interfacial tension between them is higher for the hydrophilic resin ($\gamma_{12} \sim 12$ mN/m) than for the hydrophobic one ($\gamma_{12} \sim 10$ mN/m) [38]. In addition, the size of the droplets of the hydrophilic alkyd resin was smaller than that of the hydrophobic alkyd, (S1630, $d_d = 640$ nm and S293, $d_d = 900$ nm), namely the interfacial area between the alkyd resin and acrylic polymer was higher for the hydrophilic resin. Therefore, the driving force for phase migration was higher for the blend containing the hydrophilic resin, and this explains the larger size of the alkyd aggregates in the film cast from the blends containing the hydrophilic resin (Fig. 2).

The hybrid contained up to three phases: alkyd resin, grafted copolymer and acrylic polymer. Table 1 presents the fractions of these polymers in each hybrid. It can be seen that hybrid S1 contained 66.5 wt% of grafted polymer, 5.5 wt% of acrylic polymer and 28 wt% of alkyd resin. As the interfacial tensions between the grafted polymer and both acrylic polymer and alkyd resins are lower than that between the acrylic polymer and the alkyd resin, the driving force for phase migration is lower than for the blends. On the other hand, migration is favored by the presence of low molecular weight polymer, which was in a relatively low amount in hybrid S1. Therefore, this system had a relatively low driving force for phase migration and a relatively low amount of mobile free alkyd resin. In addition, the fact that the alkyd resin occupied the core of the polymer particle might offer some resistance to alkyd migration. The combination of these effects resulted in a moderate phase separation. On the other hand, as compared with hybrid S1, hybrid S3 contained a lower fraction of grafted copolymer (35.5 wt %) and higher fractions of acrylic polymer (25 wt%) and alkyd resin (39.5 wt%). Therefore, it had a stronger driving force for phase

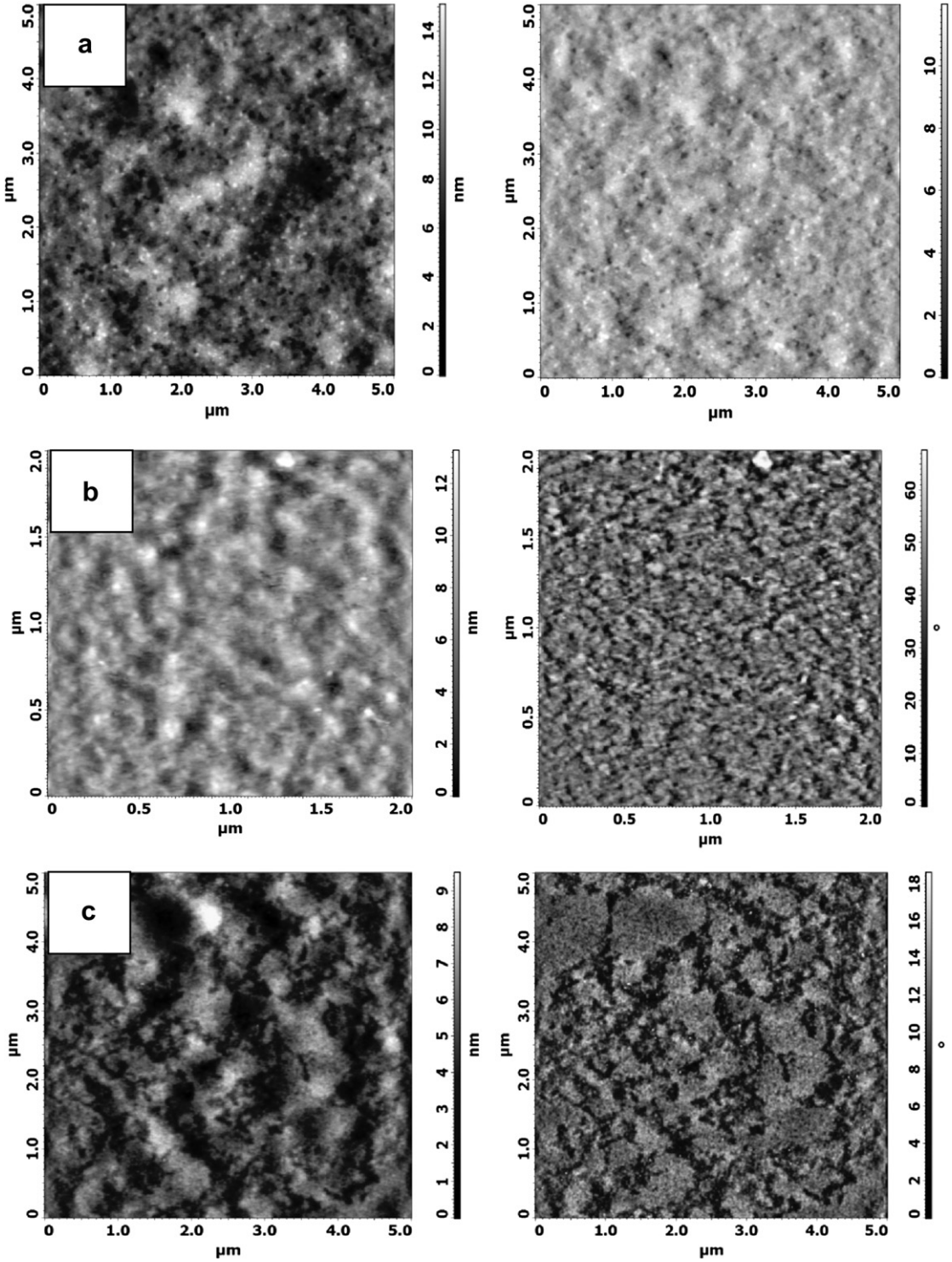

Fig. 3. AFM images of top air surface of (a) S1, hydrophobic S293 resin with BA; (b) S2, hydrophobic S293 resin with BMA; (c) S3, hydrophilic S1630 resin with BA. Height images are shown on the left and phase images are shown on the right. Dark regions correspond to the alkyd rich phase and bright regions to the acrylic-rich phase.

migration and a higher amount of the more mobile phase (alkyd resin), which provide reasons for the larger aggregates of alkyd resin formed in the films. The formation of the aggregates was facilitated by the location of the alkyd in the exterior of the particle (Fig. 1). In addition, this hybrid had also the smallest particle size, and hence a higher interfacial area among the phases, which may contribute to increase the driving force for phase migration.

The properties of hybrid S2 in terms of polymer microstructure and particle morphology were intermediate between hybrids S1 and S3, and hence the extent of phase separation (Fig. 3) was also intermediate.

The results discussed above show that phase migration leading to the formation of aggregates increases when (1) the fraction of low molecular weight polymer (free alkyd resin) increases, (2) the

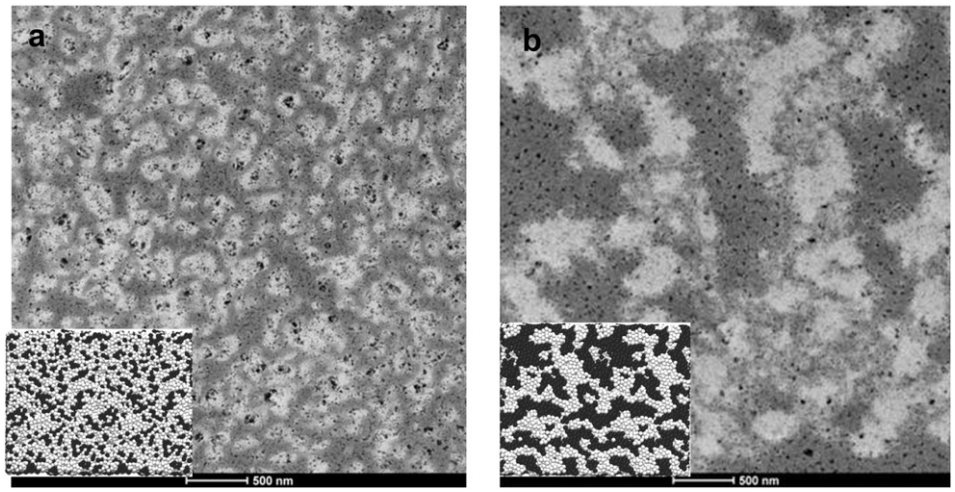

Fig. 4. TEM micrographs of film cross-sections of (a) S1, containing S293 resin and (b) S3, containing S1630 resin. Scale bar 500 nm. Dark regions correspond to the alkyd rich phase and bright regions to the acrylic-rich phase.

compatibility between the phases decreases (smaller fraction of grafted copolymer), and (3) when the more mobile phase (alkyd resin) is located at the outer part of the particles.

The contributions of the polymer characteristics and particle morphology cannot be decoupled because in these and other hybrids, the system with the higher driving force for phase migration presents the more favorable particle morphology for phase migration. Unfortunately, for the present system, synthesis of hybrids that present counteracting characteristics for phase migration (e.g., hydrophilic resin in the core of the particles) is very difficult, if not impossible.

The understanding of the relative importance of the polymer characteristics and the particle morphology, as well as the application of this knowledge to other systems would both benefit from computer simulations of the phase migration during film formation. Therefore, a standard coarse-grained canonical Monte Carlo model aimed at predicting the morphology of the film was developed.

3.1. Modeling the formation of film morphology

Because the morphology of the waterborne hybrid particles was at thermodynamic equilibrium, they were not subjected to any significant driving force for phase migration while they were surrounded by water. Therefore, phase migration was presumed to occur after completion of water evaporation, and in the simulation, the film after water evaporation was considered to be formed by particles randomly distributed in a dense packing. Although the hybrid particles may contain three components (acrylic polymer, grafted copolymer and free alkyd), only two phases were considered in the simulation: free alkyd resin and acrylic containing polymer. This assumption is based on the following three reasons: (i) the grafted copolymer was richer in the acrylic polymer than in alkyd resin and it is expected to be compatible with the pure acrylic polymer; (ii) the low molecular weight alkyd resin is expected to be more mobile than the high molecular weight acrylic containing polymer (both pure and grafted [40]); and (iii) the available AFM and TEM images only distinguished between acrylic-rich and alkyd rich domains.

Both cluster migration and diffusion of individual polymer chains contribute to the evolution of the film morphology. There are no data available for the kinetics of film morphology, but the results available for the dynamics of the particle morphology indicate that cluster migration is the main contribution in such a case [34–36]. For the current case, the large size of the clusters and the relatively low molecular weight of the alkyd resin may increase the significance of the diffusion. In order to model such a complex system, the polymer chains contained in each polymer particle were pulled together in a number of beads and the beads were allowed to move in the film. The beads were larger than single polymer chains and smaller than the size of the clusters, therefore they may represent the average motion of the polymer in the system. The interaction among the beads was simulated using a Lennard-Jones potential because it captures well the main contributions (Bohr repulsion and van der Waals attraction) to the movement and, although developed for small molecules, it has been successfully used to simulate colloid–colloid interactions [49–51].

Each composite particle was considered to be composed by 25 subparticles, each of them corresponding to either free alkyd resin or acrylic containing polymer. The distribution of the subparticles between these polymers was made by taking into account the resin degree of grafting of the hybrids. In addition, the experimental particle morphology (Fig. 2) was accounted for. Fig. 5 presents the model considered for the hybrid particles. Hybrid S1 had a core-shell morphology with 7 subparticles representing the alkyd in the core (28% of the total polymer) and 18 subparticles representing the acrylic-rich phase in the shell (72% of the total polymer). The choice of the number of subparticles affects the aspect of the polymer particle. Thus, a higher number of subparticles would result in a better coverage of the alkyd core by the acrylic shell.

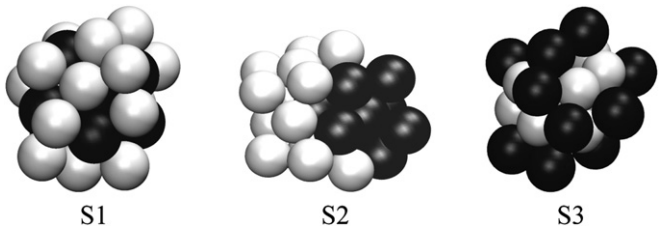

Fig. 5. Schematic morphologies of the polymers particles used in the simulation. The black subparticles represent the alkyd phase while the white ones represent the acrylic containing polymer.

However, the computational time would tremendously increase. Therefore, each polymer particle was represented by 25 subparticles.

Hybrid S2 had a hemispherical morphology with 10 subparticles representing the pure alkyd resin (41% of the total polymer) and 15 subparticles representing the graft copolymer (no pure acrylic polymer was detected in this case). Although hybrid S3 was the only system that contained 3 phases in similar amounts, in the simulation, it was considered that the particle was composed by 13 alkyd subparticles that surrounded a core of 12 acrylic subparticles, i.e., the hybrid polymer was shared between the pure alkyd and the acrylic phases.

The initial configuration of the film was obtained by randomly distributing the hybrid particles (each of them composed of 25 subparticles) within the simulation cell without overlapping and maintaining the particle morphology.

In the simulation, the following interactions were considered: (i) interaction among the subparticles representing the polymers, (ii) interaction among the polymer subparticles and the film/air interface, and (iii) interaction between the polymer subparticles with the substrate. The polymer–polymer interaction between two subparticles representing polymers i and j separated by a distance r, $U_{ij}(r)$, was described by a Lennard-Jones potential

$$U_{ij}(r) = 4\varepsilon_{ij}\left(\left(\frac{\sigma_{ij}}{r}\right)^{12} - \left(\frac{\sigma_{ij}}{r}\right)^{6}\right) \quad (4)$$

where ε_{ij} is the attractive depth of the potential well and σ_{ij} is the distance at which the potential is zero, which was set as $\sigma_{ij} = 1$ and used as the unit of length in the simulation. The polymer–polymer interaction was cut at $5.0\sigma_{ij}$. In the present simulations, $\varepsilon_{\text{alkyd-alkyd}} = 25$ and $\varepsilon_{\text{acrylic-acrylic}} = 30.0$, meaning that the attractive well was deeper for acrylic-rich polymers than for alkyd resins, which reflects the physical situation in which the alkyd resin could flow more easily than the acrylic/hybrid polymer due to its lower viscosity.

On the other hand, for the interaction between acrylic-rich polymers and alkyd resin, ε_{ij} was calculated as

$$\varepsilon_{ij} = \alpha\left(\varepsilon_{\text{alkyd-alkyd}}\ \varepsilon_{\text{acrylic-acrylic}}\right)^{1/2} \quad (5)$$

where $\alpha\,(0 \le \alpha \le 1)$ is an arbitrary coefficient that accounted for the compatibility between polymers. When α is lower, then the higher is the interfacial tension [52] and the lower is the compatibility between polymers i and j. Hybrids S1 and S2 had a similar content of hybrid polymer, and hence, $\alpha = 0.7$ was used for both of them. For S3, a lower value ($\alpha = 0.1$) was used, because this was the system with the lowest fraction of graft copolymer.

The interaction between the polymer i and the substrate, U_{ext}, was described by the repulsive term of a Lennard-Jones-type potential, which has been used to describe the interaction between a flat surface and particles [53].

$$U_{\text{ext}}(z_{\text{ext}}) = 4\varepsilon_{\text{ext}}\left(\frac{0.5\sigma_{ij}}{z_{\text{ext}}}\right)^{n} \quad (6)$$

where z_{ext} is the perpendicular distance between the center of the subparticle and the external interface, ε_{ext} is the attractive well of the potential, and n is a parameter that is related to the stiffness of the interface. When n is higher, then the interfacial tension is higher. In this work, $\varepsilon_{\text{ext}} = 1.0$ and $n = 6$ were used for any of the components.

Because polymer does not evaporate, the film/air interface acts as an impenetrable wall for the polymer. In the framework of the Metropolis algorithm [54] used in this work, this can be treated by ignoring the Boltzmann factor (see below) or by using a repulsive potential [7]. In this work, the repulsive potential given in Eq. (6) was used with $\varepsilon_{\text{ext}} = 1.0$ and $n = 6$. This is not expected to affect the morphology of the film surface (and obviously that of the interior of the film) because the two phases were equally affected.

The simulation cell was a parallelepiped with dimensions $L_x = L_y = 24\sigma_{ij}$ and $L_z = 40\sigma_{ij}$, L_z being the direction perpendicular to the substrate. The cell contained 760 particles and 19,000 subparticles. Periodic boundary conditions were applied in the x and y directions. In the z direction, the interaction was defined by Eq. (6).

Once the initial configuration was obtained, the subparticles that formed the polymer particle were allowed to move individually according to the Metropolis algorithm [54], which drives the system toward its equilibrium state. In this algorithm, a subparticle is chosen at random and its potential energy as a function of the position is calculated, E_{old}, through Eqs. (4)–(6). Then, the subparticle is displaced to a new random position, getting a new energy, E_{new}. If $E_{\text{new}} < E_{\text{old}}$, the new position is accepted. Otherwise, the Boltzmann factor, $\exp[-(E_{\text{new}}-E_{\text{old}})/k_BT]$ (where k_B is the Boltzmann constant and T the temperature, set as $k_BT = 1$), is calculated and compared to a random number uniformly distributed between zero and one. The new position is accepted if the random number is lower than the Boltzmann factor and rejected otherwise. The first condition assures that the system evolves toward the lowest energy, meanwhile the second condition reduces the possibility that the system freezes in a local minimum of the energy. In a Monte Carlo step, all the subparticles were tried to be

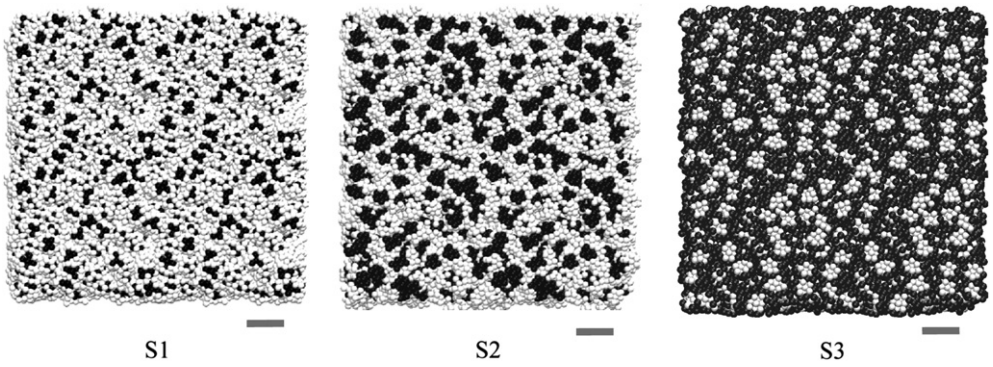

Fig. 6. Snapshots of the initial configuration of film/air surface. The scale bar is 313 nm. The black subparticles represent the alkyd phase while the white ones represent the acrylic containing polymer.

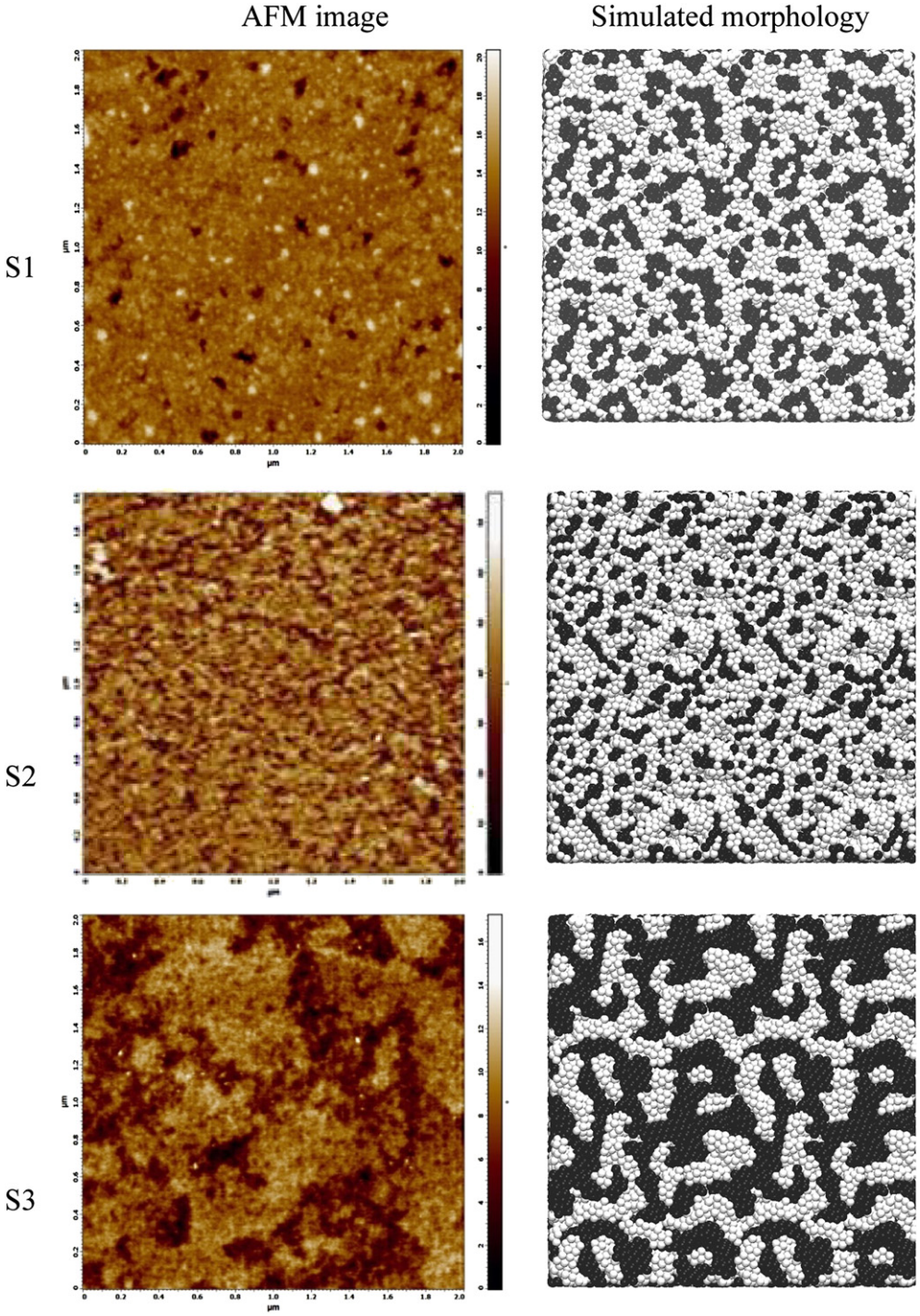

Fig. 7. Comparison of the film/air interface morphologies determined experimentally by AFM with the simulated morphologies (after 5×10^6 Monte Carlo steps). Dark brown regions represent alkyd rich phase and light brown regions the acrylic-rich phase in AFM. The black subparticles represent the alkyd phase while the white ones represent the acrylic containing polymer in the simulation. (For interpretation of the references to color in this figure legend, the reader is referred to the web version of this article.)

displaced with acceptance ratio close to 50% by adjusting the maximum length of displacement, $l = 0.012\sigma_{ij}$. In order to account for the lower viscosity of the alkyd resin, displacement of the alkyd subparticles was tried with a higher frequency ratio (2:1), with respect to the acrylic subparticles.

The evolution of the film during the simulation was analyzed with the aid of snapshots and by the normalized cluster size weight distribution of the alkyd subparticles [55], which was calculated considering that alkyd subparticles belonged to the same cluster if the separation distance between the subparticles was less than $1.05\sigma_{ij}$. For each simulation, 5×10^6 Monte Carlo steps were performed. The final film morphologies were metastable, i.e., morphologies that cannot significantly vary with the thermal energy available in the system.

Fig. 6 presents a snapshot of the initial configuration of the air-film surface for the three hybrids. The scale bar represents 313 nm and was calculated considering that the polymer particle size was 100 nm (see Table 1). The small agglomerates of alkyd resin that are

observed in the case of hybrid S1 are due to the imperfect coverage of the alkyd subparticles forming the core of the polymer particles by the acrylic subparticles, because of the limitations imposed by the number of subparticles forming a hybrid particle. The clusters of alkyd resin observed in hybrids S2 and S3 correspond to the aggregation of the alkyd from neighbor particles, because in these hybrids the alkyd resin is mainly at the exterior of the particles.

Fig. 7 presents a comparison of the simulated morphology of the film/air interface (after 5×10^6 MCS) with the morphologies determined experimentally by AFM. The size of the images was adapted in order to have the same scale in the simulated and in the AFM images. It is worth pointing out that no parameter estimation was performed. It can be seen that the simulation predicts well the trends observed experimentally, i.e., the size of the aggregates increased from S1 to S2 and S3. Quite likely, the size of the alkyd clusters was overestimated for hybrid S1 because no perfect core-shell morphology can be achieved with 25 subparticles. Regarding the system S3, it may be noted that the alkyd or acrylic aggregates in the simulated film do not appear to be as large as in the experimental AFM image. Higher segregation could be obtained by modifying the parameters of the potential and the mobility of the phases, but no parameter estimation was performed because the main objective was to demonstrate that the model was able to capture the experimental trends. In addition, due to computing limitations (the simulation was performed in a small portion of the film, 1.5 μm × 15 μm), which limited the possibility of quantitative comparison.

In Fig. 4, the simulation results and TEM micrographs of cross sections for hybrids S1 and S3 are shown. It can be seen that the model was able to predict the trends observed, as the size of the clusters was larger for hybrid S3 than for hybrid S1.

As a case study, the model was also used to explore the effect of combinations of polymer microstructure and particle morphology not attainable experimentally with the current acrylic-alkyd system. Specifically, it was used to gain some understanding about the relative importance of the polymer characteristics (extent of grafting) and the particle morphology in determining the film morphology. Therefore, using system S3 as a reference, the effect of grafting for this particle morphology on film formation was simulated using $\alpha = 0.7$ (representing higher compatibility, system S3a) for comparison to system S3 ($\alpha = 0.1$). In addition, the effect of the reversed core-shell particle morphology (alkyd in the core and acrylic in the shell) with the same number of acrylic and alkyd subparticles than System S3 was simulated for high and low grafting levels (Systems S3b, $\alpha = 0.1$; and S3c, $\alpha = 0.7$; respectively).

The simulated cross-sectioned films are presented in Fig. 8. For both particle morphologies, there is a clear difference in film structure when comparing high and low grafting. On the other hand, when there is a high level of grafting and compatibility ($\alpha = 0.7$), there is very little difference between the film morphology for S3a particle morphology and the reversed particle morphology in S3c. Hence, these simulations show that the effect of phase compatibility on film morphology appears to be stronger than that of particle morphology. However, it is worth pointing out that because of the limitations in computer time, the number of subparticles in a particle was limited to 25. Consequently, the coverage of the core by the shell was not perfect, and therefore the effect of the particle morphology on film morphology may be underestimated because of imperfections in the shell.

The developed model combined with models for particle morphology [32,34–37,56–58] is valuable for guiding future experimental work aimed at controlling the film morphology. The principles obtained from the models are applicable to other hybrid systems with differing compositions.

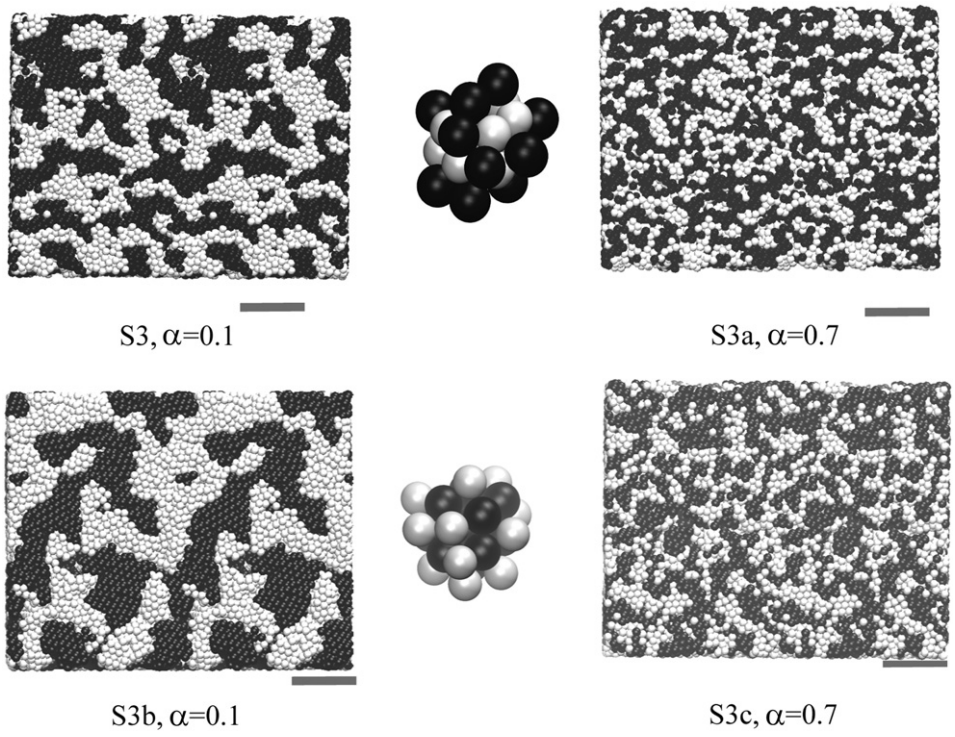

Fig. 8. Effect of the particle morphology and phase compatibility on the simulated morphology of the cross-sectioned films. The scale bar is 313 nm. The black subparticles represent the alkyd phase while the white ones represent the acrylic containing polymer. In the top row, the alkyd is in the shell and the acrylic in the core. In the bottom row, the structure is reversed, and the alkyd is in the core. In the left column, lower compatibility ($\alpha = 0.1$) is being simulated. In the right column, compatibility is higher ($\alpha = 0.7$).

4. Conclusions

Insight has been gained into how the morphology of hybrid particles is transformed into film morphology. Waterborne alkyd/acrylate hybrids were used as a case study but the concepts are more widely applicable. The hybrids contained acrylic polymer, alkyd resin and alkyd-grafted acrylic polymer that helped the compatibilization of the other two components. All the films presented aggregates of alkyd resin and acrylic-rich polymer that were larger than the size of the corresponding phase in the particles, meaning that phase migration and agglomeration occurred during the film formation. Phase migration in blends of alkyd and acrylic particles was more apparent than in the hybrid particles because of the compatibilising effect of the grafted alkyd-acrylic copolymer. The results from the hybrid systems identified three key factors that enhanced phase migration, leading to the formation of aggregates in the films. Phase migration increased as the fraction of the low molecular weight polymer (free alkyd resin) increased, as the compatibility between the phases decreased (i.e., a smaller fraction of grafted copolymer), and when the more mobile phase was located in the outer part of the particles. A standard canonical Monte Carlo model was developed to simulate the transformation of the particle morphology into film morphology. The simulation was able to predict the observed experimental trends. The model was used to gain some understanding about the relative importance of the polymer compatibility and the particle morphology. The results obtained showed that the effect of the phase compatibility on film morphology was stronger than that of the particle morphology. In combination with models for particle morphology, this model is valuable for designing strategies to control the film morphology.

Acknowledgments

The financial support received from the European Union project (Napoleon NMP3-CT-2005-011844), University of the Basque Country (Ayudas a la Especialización de Doctores), Diputación Foral de Gipuzkoa, Basque Government (GV 07/16-IT-303-07 and SAIOTEK 2010 Ref. S-PE10UN25) and Ministerio de Ciencia y Tecnología (CTQ 2006-03412 and Programa Consolider-Ingenio 2010 “CIC nanoGUNE Consolider” contract CSD2006-00053) are gratefully acknowledged. The SGI/IZO-SGIker UPV/EHU is gratefully acknowledged for allocation of computational resources.

References

[1] Asua JM. Polymeric dispersions: principles and applications. Dordrecht: Kluwer Academic Publishers; 1997.
[2] Lovell P. Emulsion polymerization and emulsion polymers. New York: Wiley-Interescience; 1997.
[3] Urban D, Takamura K. Aqueous polymer dispersions. Hoboken: John Wiley & Sons; 2002.
[4] Keddie JL. Mater Sci Eng Rep 1997;21:101–70.
[5] Steward PA, Hearn J, Wilkinson MC. Adv Colloid Interface Sci 2000;86:195–267.
[6] Keddie JL, Routh AF. Fundamentals of latex film formation: processes and properties. Dordrecht: Springer; 2010.
[7] Reyes Y, Duda Y. Langmuir 2005;21:7057–60.
[8] Schuler B, Baumstark R, Kirsch S, Pfau A, Sandor M, Zosel A. Prog Org Coat 2000;40:139–50.
[9] Directive 2004/42/CE of the European Parliament and the Council, Official Journal of the European Union.
[10] Feng JJ, Winnik MA, Shivers RR, Clubb B. Macromolecules 1995;28:7671–82.
[11] Keddie JL, Meredith P, Jones RAL, Donald AM. Langmuir 1996;12:3793–801.
[12] Eckersly ST, Helmer BJ. J Coat Technol 1997;69:97–107.
[13] Geurts J, Bouman JA, Overbeek A. J Coat Technol Res 2008;5:57–63.
[14] Colombini D, Hassander H, Karlsson OJ, Maurer FH. Macromolecules 2004;37:6865–73.
[15] Tzitzinou A, Keddie JL, Geurts JM, Peters ACIA, Satguru R. Macromolecules 2000;33:2695–708.
[16] Chevalier Y, Hidalgo M, Cavaillé JY, Cabane B. Film formation in waterborne coatings. ACS-Symposium Series 648; 1996. 244–254 [Chapter 16].
[17] Juhué D, Lang J. Macromolecules 1995;28:1306–8.
[18] Lee DI. J Polym Sci Part A Polym Chem 2006;44:2826–36.
[19] Kirsch S, Stubbs J, Leuninger J, Pfau A, Sundberg D. J Appl Polym Sci 2004;91:2610–23.
[20] Gerharz B, Kuropka R, Petri H, Butt HJ. Prog.Org Coat 1997;32:75–80.
[21] Schellenberg C, Akari S, Regenbrecht M, Tauer K, Petrat FM, Antonietti M. Langmuir 1999;15:1282–90.
[22] Hagen R, Salmen L, Karlsson O, Wesslen B. J Appl Polym Sci 1996;62:1067–78.
[23] Lee DY, Park YK, Khew MC, Ho CC, Kim JH. Macromol Symp 2000;151:479–85.
[24] Otts DB, Pereira KJ, Jarret WL, Urban MW. Polymer 2005;46:4776–88.
[25] Deriss MJ, Karlsson OJ. Surf Coat Int Part B-Coat Trans 2005;88:251–6.
[26] Colombini D, Deriss MJ, Karlsson OJ, Maurer FHJ. Macromolecules 2004;37:2596–602.
[27] Mallégol J, Barry AM, Ciampi E, Glover PM, McDonald PJ, Keddie JL, et al. J Coat Technol 2002;74:113–24.
[28] Nabuurs T, Baijards RA, Germa AL. Prog Org Coat 1996;27:163–72.
[29] Wu XQ, Schork FJ, Gooch JW. J Polym Sci Part A: Polym Chem 1999;37:4159–68.
[30] Van Hamersveld EMS, Van Es J, Cuperus FP. Colloids Surf A 1999;153:285–96.
[31] Tsavalas JG, Luo Y, Hudda L, Schork FJ. Polym React Eng 2003;11:277–304.
[32] de la Cal JC, Urzay R, Zamora A, Forcada J, Asua JM. J Polym Sci Polym Chem 1990;28:1011–31.
[33] Chen YC, Dimonie V, El-Aasser MS. Macromolecules 1991;24:3779–87.
[34] González-Ortiz LJ, Asua JM. Macromolecules 1995;28:3135–45.
[35] González-Ortiz LJ, Asua JM. Macromolecules 1996;29:383–9.
[36] González-Ortiz LJ, Asua JM. Macromolecules 1996;29:4520–7.
[37] Sundberg DC, Durant YG. Polym React Eng 2003;11:379–432.
[38] Goikoetxea M, Minari R, Beristain I, Paulis M, Barandiaran MJ, Asua JM. J Polym Sci Part A: Polym Chem 2009;47:4871–85.
[39] Van Hamersveld EMS, Van Es JJGS, German AL, Cuperus FP, Weissenborn P, Hellgren AC. Prog Org Coat 1999;35:235–46.
[40] Wang T, de Las Heras C, Goikoetxea M, Beristain I, Paulis M, Barandiaran MJ, et al. Langmuir 2010;26:14323–33.
[41] Minari RJ, Goikoetxea M, Beristain I, Paulis M, Barandiaran MJ, Asua JM. J Appl Polym Sci 2009;114:3143–51.
[42] Minari RJ, Goikoetxea M, Beristain I, Paulis M, Barandiaran MJ, Asua JM. Polymer 2009;50:5892–900.
[43] Immergut EH, Bandrup J, Grulke EA. Polymer handbook. 4th ed. NewYork: John Wiley & Sons; 1999.
[44] Koenig AM, Weerakkody TG, Keddie JL, Johannsmann D. Langmuir 2008;24:7580–9.
[45] Goicoechea M, Barandiaran MJ, Asua JM. Macromolecules 2006;39:5165–6.
[46] Anczykowski B, Gotsmann B, Fuchs H, Cleveland JP, Elings VB. Appl Surf Sci 1999;140:376–82.
[47] Scott WW, Bhushan B. Ultramicroscopy 2003;97:151–69.
[48] Lei C, Ouzineb K, Dupont O, Keddie JL. J Colloid Interface Sci 2007;307:56–63.
[49] Dzwinel W, Yuen DA. J Colloid Interf Sci 2000;225:179–90.
[50] Dzwinel W, Yuen DA, Boryczko K. J Mol Model 2002;8:33–43.
[51] Guzman O, de Pablo JJ. J Chem Phys 2003;118:2392–7.
[52] Diaz-Herrera E, Ramírez-Santiago G, Moreno-Razo JA. J Chem Phys 2005;123:184507/1–184507/9.
[53] Duda Y, Lara-Ochoa F, Trokhymchuk A. Colloids Surf A 2000;161:477–88.
[54] Landau DP, Binder KA. Guide to Monte Carlo simulations in statistical physics. 2nd ed. Cambridge: Cambridge University Press; 2005.
[55] Sevick EM, Monson PA, Ottino JM. J Chem Phys 1988;88:1198–206.
[56] Reyes Y, Asua JM. J Polym Sci Part A Polym Chem 2010;48:2579–83.
[57] Reyes Y, Paulis M, Leiza JR. J Colloid Interface Sci 2010;352:359–65.
[58] Akhmatskaya E, Asua JM. J Polym Sci Part A Polym Chem, in press.